Nanoscale

PAPER

View Article Online
View Journal | View Issue

Cite this: *Nanoscale*, 2024, **16**, 1320

Dual functionalized copper nanoparticles for thermoplastics with improved processing and mechanical properties and superior antibacterial performance†

Lulu Tian,[a,b] Li Sun,[a] Bo Gao,[a] Fei Li,[a] Chaoran Li,[c] Ruoyu Wang,[d] Yanfang Liu,[d] Xiaohong Li,[a,b] Liyong Niu *[a,b] and Zhijun Zhang*[a,b]

The utilization of metal nanoparticles for antibacterial thermoplastic composites has the potential to enhance the safety of human and animal life by mitigating the spread and transmission of foodborne pathogenic bacteria. The dispersion, antioxidant and antimicrobial activities of metal nanoparticles directly affect the application performance of the composites. This study focused on achieving amine-carboxyl co-modified copper nanoparticles (Cu-AC) with excellent antioxidant properties and monodispersity through *in situ* grafting of amine and carboxyl groups onto the surface of copper nanoparticles *via* ligand interaction. Polyacrylic acid's extended carbon chain structure was utilized to improve its dispersion and antioxidant properties, and its antibacterial properties were synergistically enhanced using secondary amines. It was found that Cu-AC possesses high antibacterial properties, with a minimum inhibition concentration of 0.156 mg mL^{-1}. Antibacterial masterbatches and their composites (polypropylene/Cu) manufactured by melt blending of polypropylene and Cu-AC exhibited excellent antibacterial rates of up to 90% and 99% at 300 ppm and 700 ppm Cu-AC, respectively. Additionally, Cu-AC bolstered the thermal degradation, processing and mechanical properties of polypropylene. The successful implementation of this product substantiates the potential applications of polypropylene/Cu composite materials across diverse industries.

Received 9th September 2023,
Accepted 5th December 2023

DOI: 10.1039/d3nr04548j

rsc.li/nanoscale

1. Introduction

According to published studies by the WHO, there are over 600 million foodborne illnesses and 420 000 related deaths globally each year.[1,2] Foodborne bacterial pathogens are the most common cause of foodborne illness or foodborne disease worldwide.[3] The common strains, such as *Escherichia coli* (*E. coli*), mould, *Staphylococcus aureus* (*S. aureus*), and Salmonella, are present throughout food production, processing and storage as well as the living environment.[4,5] Antibiotics have traditionally been used to combat these bacteria, but their overuse has led to antibiotic resistance, posing a serious threat to the health of humans and animals.[6] In order to reduce the use of antibiotics and combat pathogenic bacteria, broad-spectrum antibacterial agents and antibacterial thermoplastic composites can be used to prevent their reproduction and spread.[7–9] These composites are cost-effective and light weight, and their development and application will significantly improve the safety of human and animal life.

Silver and copper nanoparticles, due to their small size, high surface activity and broad-spectrum antibacterial properties, are widely used as antibacterial agents in coatings, plastics and other materials to protect them from microbial attack.[10–17] Among them, copper nanoparticles are not only inexpensive and less biotoxic, but also have better antibacterial properties than silver nanoparticles.[18–23] In addition, copper plays an important role in human metabolism as one of the important trace elements and an essential cofactor of metalloproteins.[24] Copper nanoparticle-based antimicrobial agents are expected to replace Ag nanoparticle-based antibacterial agents and expand the scope of composite applications. The disadvantage of copper nanoparticles is that their high activity makes them prone to agglomeration and oxidation, which greatly limits their application.[25,26] Therefore, surface modifi-

[a]*Engineering Research Center for Nanomaterials, Henan University, Kaifeng 475004, China. E-mail: ly.niu2016@vip.henu.edu.cn, zhangzhijun@henu.edu.cn*
[b]*Engineering Research Center for Nanomaterials Co., Ltd, Henan University, Jiyuan 459000, China*
[c]*State Key Laboratory of Crop Stress Adaptation and Improvement, Henan University, Kaifeng 75004, China*
[d]*Zhengzhou Lingyu New Material Co., Ltd, Zhengzhou 450100, China*
† Electronic supplementary information (ESI) available. See DOI: https://doi.org/10.1039/d3nr04548j

cation of copper nanoparticles *via* grafting organic molecules is an effective way to improve their application performance.[27–29] This technique can establish a spatial site barrier, effectively curbing agglomeration, mitigating oxidation and concurrently restricting particle size. Currently, various types of surface-capping agents including polymers, acids, amines, bromides, ligands, thiols and silicates are commonly used for the modification of copper nanoparticles.[30] Specifically, grafting polymer modifiers with long carbon chain structures, akin to those present in polymer resin materials, onto the surface of copper nanoparticles proves advantageous for enhancing their dispersion in polymer resins. Moreover, the antimicrobial efficacy of antibacterial nanoparticles and polymers is influenced by the structure of different amine groups.[31–33] Notably, homopolymers with secondary amine groups demonstrate optimal performance in this regard.[34] It is reasonable to speculate that imparting long carbon chains and secondary amine group structures to copper nanoparticles will confer better antimicrobial properties.

Antimicrobial agents have the capacity to modify polymers, resulting in the formation of antibacterial composites. This enables the incorporation of pathogen-inhibiting properties into various environmental components, thereby significantly improving the safety of human and animal life. Polymer melt blending represents a widely adopted approach for polymer modification, offering ease of processing and unlimited opportunities to produce materials with versatile properties.[35] Through melt blending with copper nanoparticles, antibacterial thermoplastic composites can be synthesized. However, the limitations of physical blending can give rise to aggregation during the mixing process, thereby affecting the resulting application properties.[36] To address this challenge, secondary blending and dilution of high concentration copper masterbatches can be employed to effectively ameliorate the agglomeration phenomenon associated with copper nanoparticles, ensuring their superior application performance.[37]

In order to achieve precise control over the particle size and uniformity of copper nanoparticles, this study employs a dual functionalization technique involving secondary amines and polycarboxylic acids as modifiers to concurrently modify amine and carboxyl groups. By leveraging the vacant orbitals and facile ligand coordination of copper, this approach capitalizes on the synergistic antimicrobial effect resulting from the incorporation of secondary amine groups. Furthermore, the inclusion of a long carbon chain structure within polyacrylic acid serves to enhance the binding affinity between the resin molecular chains and copper nanoparticles, thereby improving the dispersion of copper nanoparticles in the resin matrix. Also, composites are generally prepared by melt blending and dilution of high concentration copper masterbatches to ensure better dispersion of copper nanoparticles in the polymer. Given the significant growth of polypropylene (PP) as one of the primary synthetic resins, this paper specifically focuses on probing the influence of copper nanoparticles on the structure and properties of antibacterial thermoplastic composites using polypropylene as a representative resin. The prepared antibacterial PP sheets exhibit remarkable efficacy against bacteria at low concentrations of copper nanoparticle additives and have demonstrated their successful application in the pig breeding industry.

Liyong Niu

Dr Liyong Niu is currently an associate professor at the Institute of Nanoscience and Engineering, Henan University. He received his PhD at The Hong Kong Polytechnic University in 2015. He is mainly engaged in research on the large-scale preparation and application of hybrid nanomaterials, including metallic micro/nano materials and thermally conductive/encapsulated spherical electronic nanofillers.

2. Experimental

2.1 Materials

Copper hydroxide ($Cu(OH)_2$) was purchased from Hubei Jusheng Technology Co., Ltd; hydrazine hydrate ($N_2H_4{\cdot}H_2O$) was purchased from Xi'an Quanyu Chemical Raw Materials Co., Ltd; alcohol (EtOH) was obtained from Mengzhou Jinsen Chemical Products Sales Co., Ltd; 32# paraffin oil was purchased from Zibo Xinjiu Rubber Additives Co., Ltd; polyacrylic acid (PAA, AR) was obtained from Tianjin Kemio Chemical Reagent Co., Ltd; and diethylamine (DEA, AR) was purchased from Tianjin Damao Chemical Reagent Factory. Unless explicitly stated, all reagents were of industrial grade and utilized without prior purification.

The polymer resins used in this study were polypropylene (PP, K8003) and polyethylene (PE, DMDA-8008) obtained from Kunlun Dushanzi Petrochemical Company. The acrylonitrile butadiene styrene copolymer (ABS, PA-757) was obtained from Qimei Industrial Co., Ltd and nylon 66 (PA66, EPR27) was obtained from Pingdingshan Shenma Engineering Plastics Co., Ltd.

2.2 Preparation of copper nanoparticles and antibacterial composites

This study presents an innovative liquid-phase one-step method for the preparation of copper nanoparticles with exceptional antioxidation, dispersion and antibacterial properties. The resulting copper nanoparticles as polymeric antibacterial fillers were utilized to form antibacterial masterbatches, films and sheets.

2.2.1 Preparation of copper nanoparticles. In order to avoid the introduction of acid ions containing heteroatoms

during the synthesis of copper nanoparticles, this study employed copper hydroxide as a precursor. Copper hydroxide (0.4 mol), PAA, DEA and 40 g of ethanol were added to a 500 mL three-necked flask, supplemented with 320 mL of pure water and stirred well to form a suspension with a copper content of 8%–10%. The suspension was heated to 80 °C and maintained at a constant temperature for 30 min, and hydrazine hydrate (15 g, 0.24 mol) was then added to the flask to react for 2 h to form a dispersion of amine-carboxyl co-modified copper nanoparticles (Cu-AC).

2.2.2 Production of the polymer/Cu masterbatch. The polymer/Cu masterbatch was prepared by distilling the Cu-AC dispersion, replacing the solvent with paraffin oil, and melt blending the Cu-AC/paraffin oil with a resin. The paraffin oil wrapped around the surface of Cu-AC also serves to impede oxygen-induced degradation. The Cu-AC dispersion was mixed with 25 g of paraffin oil and stirred at 80 °C for 30 min. The mixture was then subjected to distillation under reduced pressure to remove the aqueous ethanol solution, forming a copper nano-oil dispersion (Cu-AC oil). The polymer resin was blended with Cu-AC oil in a mass ratio of 8 : 2 and then passed through a twin-screw extruder to form the copper antibacterial masterbatch. A total of 12 heating zones of the screw were selected for co-mixing, with the heating temperature of the polypropylene composite ranging from 150 °C (inlet) to 190 °C (outlet) at a screw speed of 50 rpm. The whole melt blending process was carried out under ambient conditions and no inert gas was used to prevent the oxidation of copper. In this study, the PP/Cu masterbatch was used as a representative blend. In addition, PE/Cu, ABS/Cu and PA/Cu masterbatches were also developed according to their characteristics.

2.2.3 Antibacterial polymeric materials. Due to the similarity of plastic processing, this paper uses PP as a typical matrix. The solid contents of Cu-AC in the antibacterial films and sheets after dilution at different concentrations are 100 ppm, 300 ppm, 500 ppm, 700 ppm, 900 ppm, and 1200 ppm, and each material is denoted as PP/Cu-XXX ppm.

Antibacterial films: PP/Cu masterbatches were added to PP resin at 0.1%, 0.3%, 0.5%, and 0.7% and film blown into antibacterial films with different concentrations of copper. Blown film conditions: melt temperature 175 °C and film thickness 20 μm.

Antibacterial sheets: PP/Cu masterbatches were added to PP resin at 0.1%, 0.3%, 0.5%, 0.7%, 0.9%, and 1.2%, respectively, and compression molded into sheets. Molding conditions: molding temperature 190 °C, pressure 20 MPa, closing time 6 min, and mold thickness 1 mm.

2.3 Structural characterization

The Cu-AC dispersion was centrifuged and washed three times with ethanol, and then dried at 50 °C for 24 h. After that, it was ground into powder and finally subjected to a series of structural characterization analyses. The morphology, particle size and dispersion state of copper nanoparticles were observed using a transmission electron microscope (TEM; JEM-2100 plus, JEOL). The brittle fracture surface morphology of the polymer was studied using a scanning electron microscope (SEM; TESCAN VEGA3) at an accelerating voltage of 5 kV. The crystal structures of copper nanoparticles and copper-loaded polymers were analyzed using X-ray diffraction (XRD; DX-2700, Dandong Haoyuan Instrument, China; Cu Kα radiation, λ = 0.15418 nm; voltage: 40 kV, current: 40 mA) in the 2θ range of 10°–80°. Cu valence analyses were conducted using an X-ray photoelectron spectrometer (XPS, Thermo escalab 250XI). Relevant parameters: monochromatic Al Kα (hv = 1486.6 eV), power 150 W, 650 μm beam spot, voltage 14.8 kV, and current 1.6 A, and charge correction was performed using C 1s = 284.8 eV. The chemical characteristics of the copper nanoparticles were analyzed by Fourier transform infrared spectroscopy (ATR-FTIR; Nicolet 170sx, Thermo Fisher Scientific). The thermal performances of the copper nanoparticles, copper antibacterial masterbatch and polymer composites were measured by thermogravimetric analysis (TGA; TG209, NETZSCH) in flowing nitrogen (10 °C min^{-1}). The surface morphology of the composite sections sputtered with Au was characterized using a scanning electron microscope (SEM; Gemini SEM 500, Carl Zeiss). The thermograms of the composites were recorded by differential scanning calorimetry (DSC; DSC3, METTLER TOLEDO) ranging from 30 to 200 °C to examine the crystallization and melting behavior of the composites.

2.4 Processing and mechanical properties of the PP/Cu composite

2.4.1 Rheological properties. The shear rheological behavior of polypropylene melts was tested using a rotational rheometer (Anton Paar MCR 302e) with a round table heated parallel plate configuration. The parallel plate rotor has a diameter of 25 mm, a release spacing of 3 mm and a test spacing of 1 mm. The following test modes were employed: (1) strain scan mode: scan mode 0.1–100% and frequency 1 rad s^{-1}; (2) temperature scan: heating rate and cooling rate 2 °C min^{-1}, scan range 150–190 °C, shear strain 0.1–1%, and frequency 10 rad s^{-1}; and (3) frequency scan: scanning range 0.01–500 rad s^{-1} and shear strain 1%.

2.4.2 Tensile test. The mechanical properties of PP/Cu antibacterial sheets were evaluated according to the GB/T1040-92 standard test method for plastic tensile properties using a universal testing machine (GOTECH TCS-2000; GOTECH testing Machines Incorporation, Taiwan, China). The test was conducted at a temperature of 25 °C and a tensile rate of 10 mm min^{-1}. To ensure the accuracy and reliability of the test, five samples were tested in parallel.

2.5 Verification of antibacterial ability

In order to study the antibacterial effect of Cu-AC, in this paper, *E. coli* (ATCC 25922) was used as a representative of bacteria. The antibacterial ability of Cu-AC was determined using the minimum inhibitory concentration (MIC) and the minimum bactericidal concentration (MBC) (shown in the ESI†) and the antimicrobial effects of the prepared PP/Cu mas-

terbatches, sheets and films were tested according to the guidelines provided in GB/T21510-2008 and GB/T31402-2015.

2.5.1 Oscillation method for testing the polymer/Cu masterbatch. To perform the test, a conical flask filled with 1 g of antibacterial masterbatch, 95 mL of liquid medium and 5 mL of 10^5 CFU mL^{-1} of bacterial suspension was incubated at 37 °C while shaking for 20 h. Then, an appropriate amount of the mixture was dispersed on agar medium and incubated at 37 °C and 56% relative humidity (RH) for 24 hours to count the viable bacteria and calculate the antibacterial rate. To ensure good reproducibility and stability, three samples were tested in parallel.

2.5.2 Lamination method for testing PP/Cu sheets and films. Square samples of size 5 × 5 cm^2 were prepared using surrogate films and sheets, followed by UV sterilization for 30 min. Subsequently, 0.4 mL of bacterial suspension (10^5 CFU mL^{-1}) was added dropwise to the surface of the specimen, covered with a 4 × 4 cm^2 polyethylene film, and incubated at 37 °C and 90% RH. After 18 h of contact incubation, 20 mL of PBS solution was added, and the bacterial solution was eluted repeatedly. An appropriate amount of bacterial suspension was dispersed on agar medium and incubated at 37 °C and 56% RH for 24 h to count the viable bacteria and calculate the antibacterial rate. To ensure reproducibility and stability, three extracts of each sample were tested in parallel.

The antibacterial rate R was calculated according to eqn (1), where R represents the antibacterial rate (%), A represents the average number of recovered colonies (CFU mL^{-1}) of the control sample coming into contact with the test bacteria after a certain time, B represents the average number of recovered colonies (CFU mL^{-1}) of the test sample coming into contact with the test bacteria after a certain time:

$$R = (A - B)/A \times 100\% \quad (1)$$

3. Results and discussion

3.1 Fabrication of Cu-AC and antibacterial composites

Fig. 1 schematically illustrates the primary fabrication process of copper nanoparticles (Cu-AC) and their antibacterial composites (PP/Cu), as well as the application of the polymeric antibacterial composite and its antibacterial mechanism. The *in situ* synthesis of copper nanoparticles shown in Fig. 1a consists of three typical processes: (1) carboxyl and amine groups dissolve part of $Cu(OH)_2$ and form a water-soluble complex. (2) The water-soluble complex is preferentially reduced to form a copper nucleus, and the excess ligand is dislodged from the surface of the nucleus to participate in the dissolution of Cu $(OH)_2$ once again. (3) Accompanied by this dynamic process, copper nanoparticles with a specific size were synthesized. The dual functionalization technique endows copper nanoparticles with excellent properties. The elongated carbon chain structure of PAA creates steric hindrance, which improves their compatibility with the polymer matrix. The presence of DEA in conjunction with copper nanoparticles synergistically contributes to their antibacterial activity. Fig. 1b shows the preparation process of the PP/Cu masterbatch and PP/Cu composites. PP/Cu composites were formed by melt mixing PP/Cu masterbatches with PP resin particles, followed by compression molding or film blowing. This process can significantly improve the dispersion of copper nanoparticles within the polymer matrix. The molecular chains of the surface-modified layer of Cu-AC are entangled with the molecular chains of the polymer to form a uniformly distributed PP/Cu composite. Fig. 1c sketches out the potential antibacterial mechanism of Cu-AC, which encompasses multiple modes of action:[38–40] (1) the interaction between copper and bacterial membranes, either through physical or chemical means, leads to the destruction of these membranes; (2) copper nanoparticles generate reactive oxygen species (ROS) *via* Fenton-like reactions, which result in enzymatic and non-enzymatic mediated oxidative damage, including lipid peroxidation, protein oxidation and DNA damage; and (3) copper ions are released from the nanoparticles to disrupt bacterial membranes and penetrate them, inducing oxidative stress responses.

3.2 Structural characterization

3.2.1 Characteristics of Cu-AC. A series of copper nanoparticles with different particle sizes were synthesized by adjusting the content and ratio of amine and carboxyl modifiers. After dual functionalization, copper nanoparticles exhibited good dispersion without agglomeration and the average particle sizes of copper nanoparticles were 30 nm, 50 nm, 80 nm and 150 nm, respectively, as confirmed by TEM photographs (Fig. 2a–d). The XRD plots (Fig. 2e) reveal the characteristic diffraction peaks of Cu located at 43°, 50°, and 74° without any signs of oxidation, which corresponds to the crystal planes of Cu (111), (200) and (220), respectively. Meanwhile, the XRD plots (Fig. S1a†) of Cu-AC, stored only in self-sealing bags under ambient conditions for a duration of more than 6 months, still maintained the metallic Cu(0) without any evidence of oxidation. The Cu LMM spectrum (Fig. S1b†) had only one obvious peak of Cu(0) species at 568.2 eV, which confirmed that Cu-AC predominantly existed in the form of metallic Cu(0).[41,42] This result indicates that it has good antioxidant properties. The infrared spectra (Fig. 2f) exhibit distinct absorption peaks corresponding to the amine, carboxyl and alkyl groups in the as-prepared Cu-AC samples. Notable peaks include the telescopic vibration peak of O–H at 3450 cm^{-1}, the telescopic vibration peaks of alkyl groups at 2941 cm^{-1}, 2889 cm^{-1} and 2827 cm^{-1}, the telescopic vibration peak of C=O at 1631 cm^{-1}, the bending vibration peak of O–H at 1542 cm^{-1}, the bending vibration peak of N–H at 1450 cm^{-1}, and the C–N stretching vibration peak at 1091 cm^{-1}. These observations provide clear evidence of the successful grafting of amine and carboxyl groups onto the surface of copper nanoparticles. A comparison of the positions of the corresponding characteristic peaks associated with the C=O stretching vibration peak and the O–H bending vibration peak in PAA reveals that the characteristic peak of Cu-AC shifted to lower wavenumbers. This shift can be attributed to

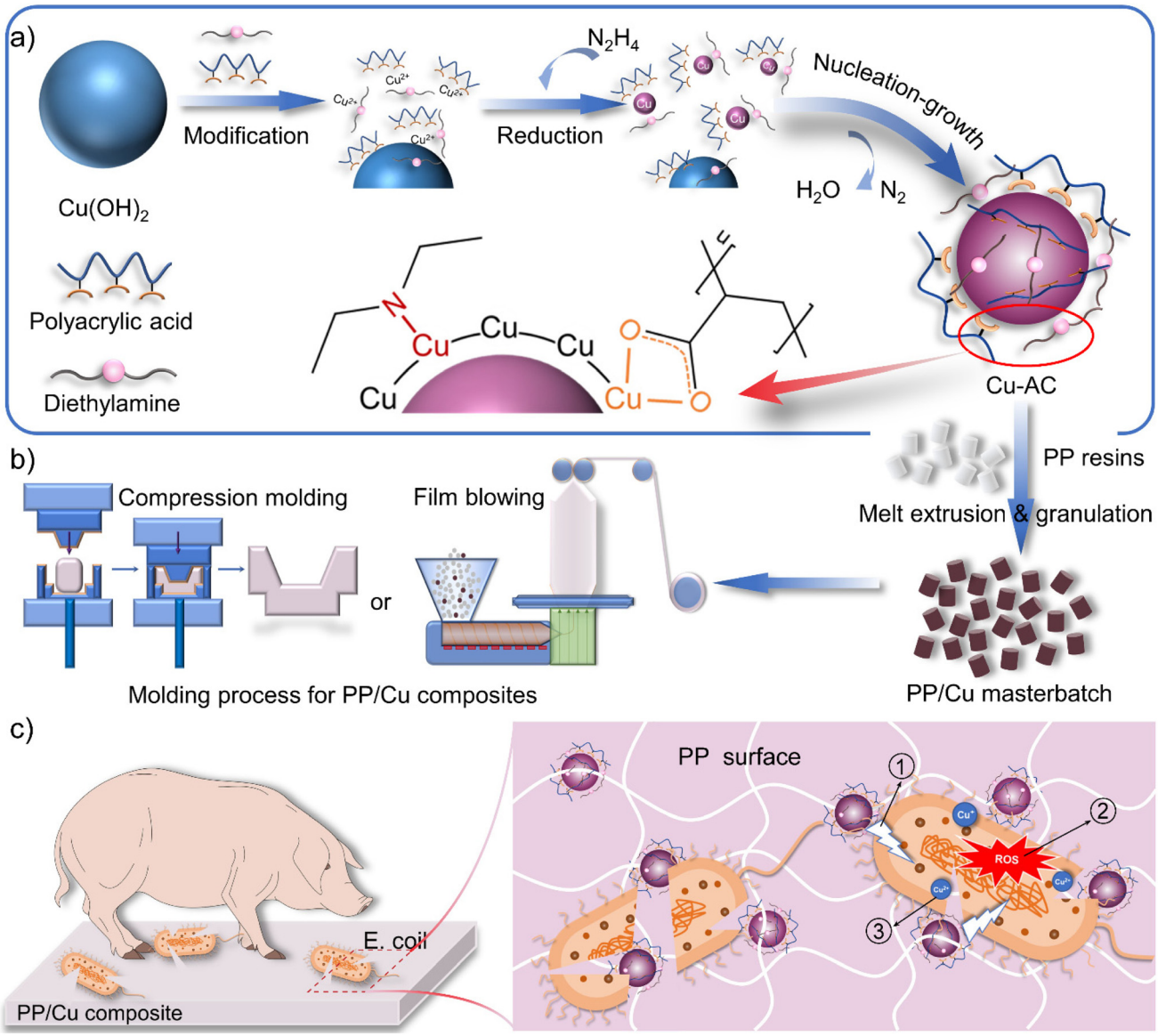

Fig. 1 Schematic illustrations of (a) the synthesis of surface-modified Cu nanoparticles and (b) melt blending for antibacterial masterbatches and their processing into composite films and sheets. (c) Schematic illustrations of the application of the polymeric antibacterial composite and its antibacterial mechanism.

the formation of a π_3^4 conjugated bond ($-COO^-$) in PAA coordinated with copper nanoparticles, which is affected by the combined effects of induction (–I) and conjugation (+C). Consequently, a reduction in the wavenumber of absorption results for the functional group.

TG plots (Fig. 2g) show two weight loss plateaus in the weight loss curves, corresponding to the decomposition of amine groups (at 95 °C) and carboxyl groups (at 260 °C), which further indicates the successful grafting of amine and carboxyl groups onto the surface of copper nanoparticles. It was also observed that as the particle size decreased, the total weight loss of the samples increased. This observation suggests that the decrease in particle size is accompanied by an augmentation of the modifier content. The presence of the modifier imparts spatial hindrance to the copper nanoparticles, thereby restraining particle growth and retarding the oxidation process.

3.2.2 Characteristics of Cu-AC in polymer resins. The dispersion of copper nanoparticles in the polymer matrix plays a crucial role in determining the processing and application properties of the thermoplastic composites. It is difficult to detect trace amounts of Cu-AC in the antibacterial composites during characterization. Therefore, the PP/Cu masterbatch was used to analyze the dispersion of Cu-AC in the resin matrix and its effect on the stability of resin materials. Cu-AC particles of size 80 nm were chosen as antimicrobial filler because they exhibited better antibacterial performance compared with Cu-AC of other particle sizes (Fig. S1c–f†). The results in Fig. S2† show

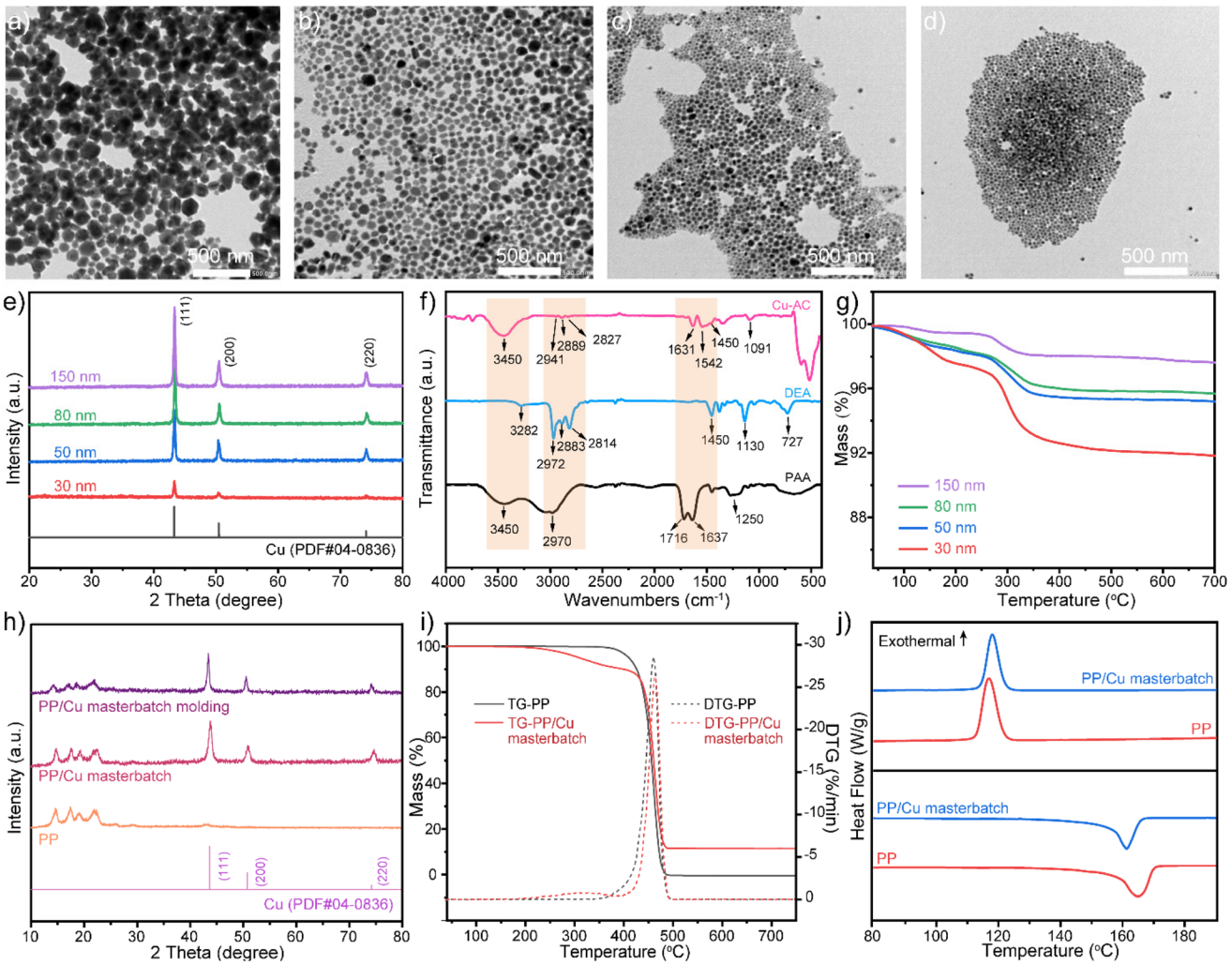

Fig. 2 (a–d) TEM photographs of copper nanoparticles; (e) X-ray diffraction patterns of copper nanoparticles; (f) FT-IR spectra of copper nanoparticles; (g) thermal weight loss curves of copper nanoparticles; (h) XRD patterns of PP and the PP/Cu masterbatch; (i) thermal loss characteristics of PP and the PP/Cu masterbatch; (j) DSC cooling and melting thermograms of PP and the PP/Cu masterbatch.

that Cu-AC in the brittle part of the composite exhibits good dispersion without aggregation even when added at high concentration (10 wt%). The oxidation resistance of copper nanoparticles at high temperature can significantly affect the application performance of the material. Therefore, XRD testing was conducted to determine whether the oxidation of Cu-AC occurred during high temperature melt blending and compression molding. As shown in Fig. 2h, Cu-AC did not exhibit the characteristic diffraction peaks of CuO and Cu_2O during the high temperature processing, but the characteristic diffraction peaks of Cu are still maintained, which indicates that it has excellent antioxidant properties.

To evaluate the effect of Cu-AC on the thermal degradation behavior of the PP matrix, we summarized and analyzed the temperature of characteristic inflection points during thermal degradation of the samples, presenting the findings shown in Fig. 2i. The weight loss curve of pure PP shows a single thermal decomposition phase, in contrast to the PP/Cu curve which shows two distinct stages of weight loss. The results suggest that the first stage of weight loss in PP/Cu is mainly attributed to the decomposition of paraffin oil, while the second stage is attributed to the degradation of PP. By comparing the second stage of weight loss of PP/Cu with that of pure PP, it was found that all three characteristic temperatures showed a shift toward higher values, accompanied by a deceleration in the thermal degradation rate. This indicates that the addition of copper nanoparticles improved the thermal degradation stability of PP. Furthermore, in combination with the decomposition trend of the modification layer of Cu-AC (Fig. 2g), the melt blending temperature of the PP/Cu composite (190 °C max.) is lower than the decomposition temperature of the modification layer on the surface of Cu-AC, which suggests that the entanglement of the modification layer with the molecular chains of PP still exists during the blending process. This improvement can be ascribed to two primary factors: (i) Cu-AC exhibits good dispersion within PP, and its

surface modification layer intertwines with the PP molecular chain, resulting in a strong interaction force between PP and Cu-AC and (ii) Cu-AC impedes the diffusion of PP decomposition products.

The melting and crystallization processes of composites have a large impact on their processing and mechanical properties. According to the DSC curves of PP/Cu, shown in Fig. 2j, the addition of Cu-AC increases the crystallization temperature and decreases the melting temperature, thus enhancing the mechanical and processing properties of PP/Cu.

3.3 Processing performance

To gain insights into the impact of copper nanoparticles on the intrinsic characteristics of the polypropylene matrix and its processing properties during high temperature melt mixing, dynamic rheological tests were performed. The high temperature melt mixing process involves both viscous flow and elastic deformation,[43] and these tests provided evidence of the influence of Cu-AC on the system. The results are displayed in both 3D plots (Fig. 3) and 2D plots (Fig. S3†). Amplitude scanning tests were employed to determine the linear viscoelastic region of the composites. Fig. 3a shows that the energy storage modulus (G') of the composites exhibited a decreasing trend followed by an increasing trend as the addition of Cu-AC increased. The linear viscoelastic zone of the composites also slightly widens with the increase of Cu-AC. This observation can be attributed to the stress imposed by Cu-AC on the polymer chains, which leads to a reduction in internal friction and enhanced motility, thus resulting in the expansion of the linear viscoelastic range platform. Subsequent temperature scan and frequency scan tests were performed within its linear viscoelastic zone of 0.1–1% and 1% strain. The blending temperature is an important parameter for polymer processing. The temperature scan (Fig. S3d† and Fig. 3b) revealed that the modulus and viscosity of the composites increased as the temperature decreased, and the composites containing Cu-AC exhibited lower modulus and viscosity compared to pure PP. By comparing the changes in the modulus and viscosity of the composites with varying amounts of Cu-AC, Fig. S3d† reveals that the intersection of the energy storage modulus and loss modulus shows a tendency to move to the low temperature region, indicating that the melting temperature of PP is lowered, which is favorable for processing at lower temperatures. This result is consistent with the DSC analysis. Fig. 3b illustrates that the viscosity of the composite initially decreased and then slightly increased with increasing copper nanoparticle content in each temperature range, but is generally lower than that of pure PP. The low-viscosity melt exhibits high fluidity, which makes it easier to process and reduces the processing energy and outlet pressure. In the frequency scan mode, as shown in Fig. 3c, the viscosity of the composite decreased with increasing shear rate, exhibiting shear-thinning behavior of a pseudoplastic fluid. Meanwhile, the addition of Cu-AC reduced the viscosity of the composites in the melting state. The behavior of Cu-AC to improve the pro-

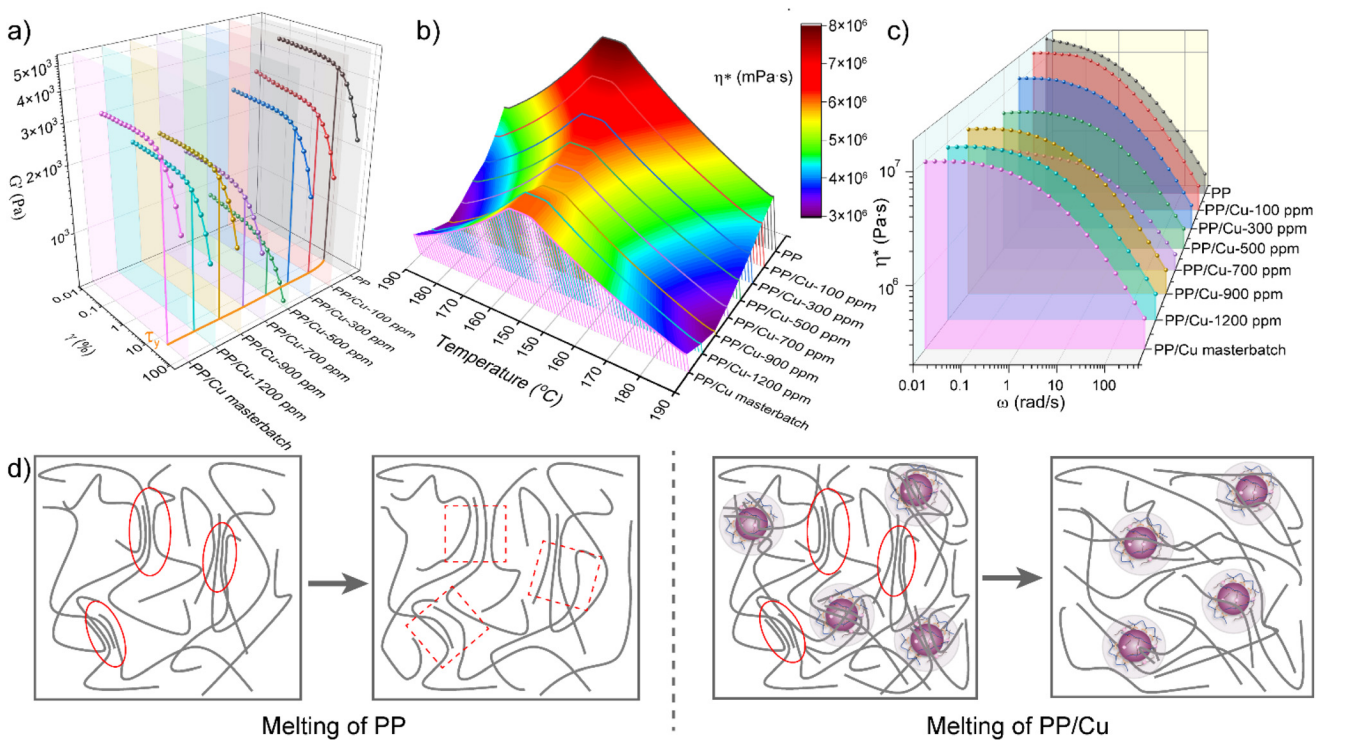

Fig. 3 Rheological performances of PP and PP/Cu composites. (a) Variation curves of modulus with strain in strain scan mode; (b) variation curves of complex viscosity with temperature in temperature scan mode; (c) variation curves of complex viscosity with angular velocity in frequency scan mode; (d) schematic illustrations of molecular chain movement within PP and the PP/Cu composite during the melting process.

cessing performance can be attributed to the role of Cu-AC as a plasticizer as shown in Fig. 3d. The incorporation of Cu-AC within the PP molecular matrix attenuates the intermolecular forces among PP chains. As a result, it shortens the necessary time for PP nuclei to disentangle molecular chains, promotes interchain slippage, and increases the overall mobility of PP molecular constituents. Simultaneously, the excellent thermal conductivity of Cu-AC expedites the thermal conduction within the composite, further facilitating the movement of molecular chains.

3.4 Mechanical properties

The mechanical properties of polypropylene composites are crucial for their performance and durability. Fig. 4 shows the tensile properties of PP/Cu composites, including their tensile strength, yield strength, yield point and elongation at break. The tensile strength, yield points and yield strengths of the PP/Cu composites increase with the addition of Cu-AC (Fig. 4a). This is because the surface modification layer of copper nanoparticles forms a core–shell structure, where the molecular chains of the shell layer entangle with the molecular chains of PP, forming an elastic interface (Fig. 4c). When the composite material is stressed, stress concentration points can form around the copper nanoparticles, which deform the elastic interface between them and PP. This prompts the shell layer of copper nanoparticles to yield and deform over a larger area, thus consuming most of the energy, resulting in an increase in the yield strength and tensile strength. The comparative elongation at break trend (Fig. 4b) shows that the elongation at break of the PP/Cu composites is greater than that of PP in the range of 100–1200 ppm of Cu-AC addition, and it exhibits an increasing and then decreasing trend with increasing amounts of Cu-AC. The reason for this phenomenon is speculated to be the elastic interface of Cu-AC enhancing the mutual interfacial interaction with PP (Fig. 4c). When the composite was deformed by the force, the stress transferred by Cu-AC drove the PP molecular chains to slip, thus increasing the plasticity of PP/Cu composites and showing an increase in elongation at break. However, as the Cu-AC nanoparticles are rigid and the PP matrix has a difference in elasticity, the stress concentration point increases with their addition, causing the material to exhibit a decreasing trend in elongation at break. Therefore, the presence of copper nanoparticles can enhance the mechanical properties of the PP composites and indirectly increase the service life of the material.

3.5 Antibacterial properties

In this study, antibacterial composite materials loaded with Cu-AC were prepared by the masterbatch dilution method. Initially, various polymeric masterbatches, including PE, PP,

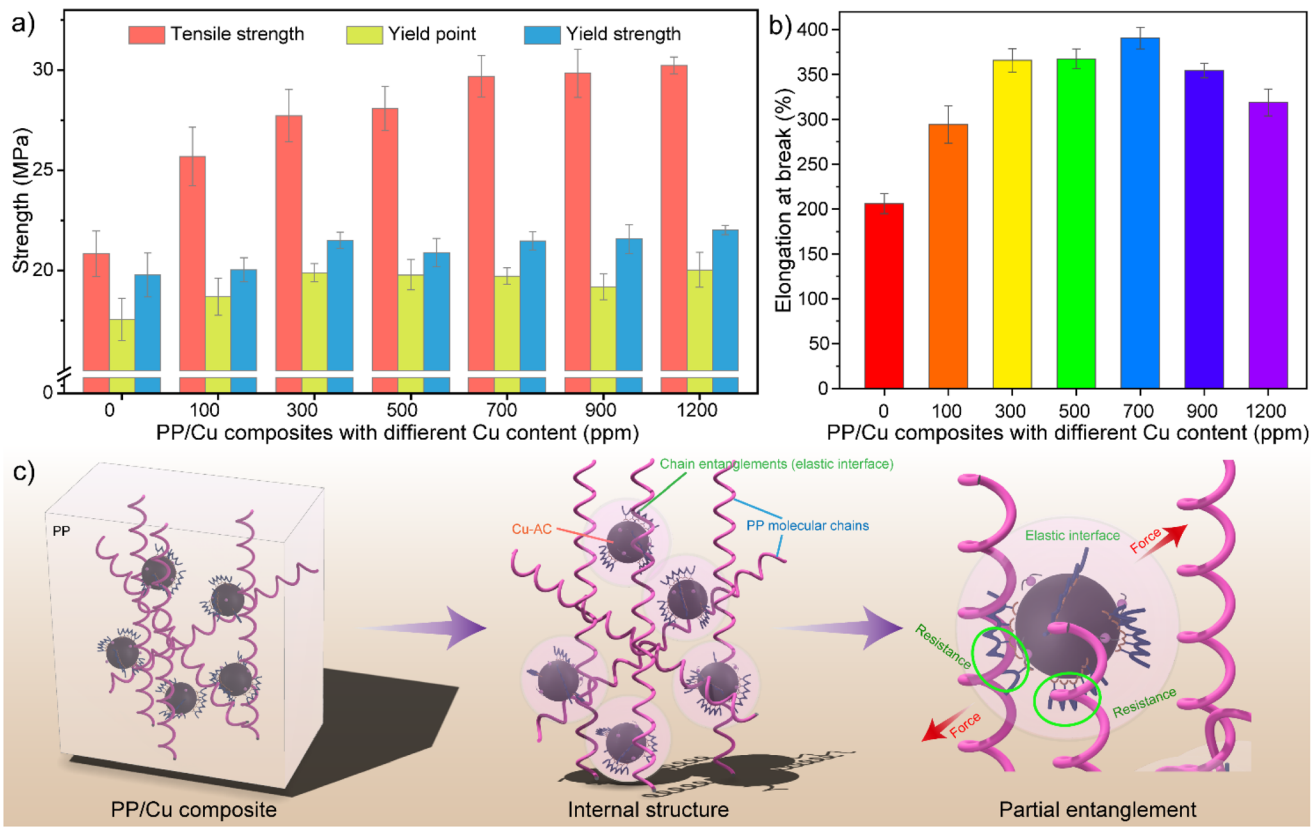

Fig. 4 Mechanical properties of PP/Cu composites. (a) Strength of PP/Cu composites as a function of Cu-AC addition. (b) Elongation at break with Cu-AC additions. (c) Schematic illustrations of the interfacial action between Cu-AC and the PP matrix.

ABS, and PA66 were synthesized by melt extrusion and granulation with the addition of 10 wt% Cu-AC nanoparticles. The antibacterial efficacy of these polymer masterbatches was evaluated, and they all exhibited excellent antibacterial performances of up to 99.9% (Fig. 5a). As an example, the Cu/PP masterbatch was selected to prepare the antibacterial composite. The addition of Cu-AC nanoparticles in the range of 100–1200 ppm was determined based on MIC and MBC test results of copper nanoparticles. The antibacterial properties of the resulting antibacterial composites, in the form of sheets and films, were then evaluated. As shown in Fig. 5b and c, a progressive increase in the antibacterial rate when increasing the content of copper nanoparticles is illustrated. Even at 100 ppm of copper nanoparticles, the antibacterial sheet and film composites displayed some degree of antibacterial activity, corresponding to the MIC value of Cu-AC. When the copper nanoparticle content exceeded 300 ppm, the surface antimicrobial rate of the composites surpassed 90%, thus achieving a class II antibacterial effect. Notably, at a copper nanoparticle content of 700 ppm or higher, the surface antibacterial activity exceeded 99%, indicating exceptional antibacterial performance and attainment of a class I antibacterial effect. When the surface antibacterial rate of the composite material reaches more than 99%, the amount of Cu-AC added corresponds to its MBC value. Consistent results were obtained from the samples collected from different regions, indicating the homogeneous dispersion of Cu-AC within PP and its consistent and reliable role in conferring antibacterial activity. This distribution state of Cu-AC in PP is further evidenced by the SEM mapping image presented in Fig. 5b. In order to illustrate the antibacterial performance of the Cu-AC and PP/Cu composites described in this study, a comparative analysis was conducted with relevant literature reports. Fig. 5d depicts the antibacterial properties of PP-based antibacterial composites with various antibacterial agents, including metals, oxides, metals/oxides, *etc.*, along with the concentrations of antibacterial agents.[14,15,21,44–48] Apparently, the copper nanoparticles and their antibacterial composites synthesized by the method described herein are characterized by low copper addition and high antibacterial activity.

Based on the experimental procedures and test outcomes of the PP/Cu composite material described in this study, we

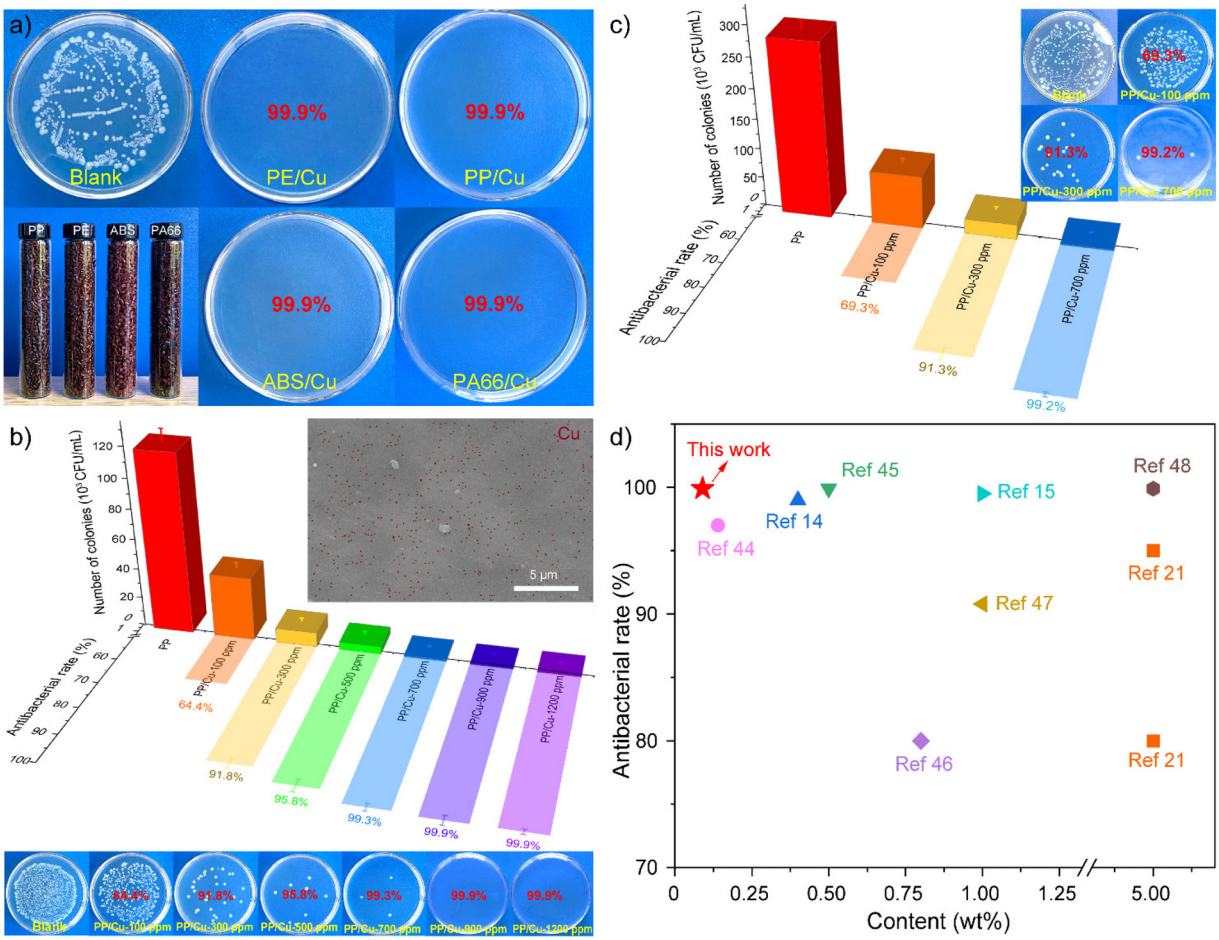

Fig. 5 (a) Culture photographs of antibacterial masterbatches after antimicrobial testing and an optical photograph of PP/Cu antibacterial masterbatches. Statistical chart of the viable bacteria number and antibacterial rate of the PP/Cu composite after bacterial culture: (b) sheets and (c) films. (d) Comparison of the antibacterial performances of PP-based antibacterial composites fabricated in this work and those reported elsewhere.

developed a specialized mold for the creation of a poultry manure leakage plate using the PP/Cu composite material (Fig. S4†). Employing the compression molding technique, we successfully produced antibacterial PP/Cu dung leaking boards, which are currently being utilized in piglet farms. According to the cost implications and incorporation amount of Cu-AC, it is postulated that the price escalation of PP/Cu composites amounts to a mere 1.5–2% per ton, thereby exhibiting a notable competitive edge in terms of pricing. The inclusion of copper nanoparticles in the composite material has endowed it with remarkable antibacterial characteristics, which renders it an excellent choice for applications requiring hygienic surfaces. The use of PP/Cu dung leaking boards has proven to be effective in preventing bacterial proliferation and curtailing the transmission of diseases in piglet farms, thereby improving the health and productivity of animals. The successful implementation of this product serves as a testament to the potential applications of PP/Cu composite materials across diverse industries.

4. Conclusion

This study reports the synthesis of copper nanoparticles with excellent antioxidant, monodispersant and antibacterial properties *via* a one-step method combined with *in situ* surface modification techniques. By grafting diethylamine and polyacrylic acid onto the surface of copper nanoparticles, we successfully endowed PP with excellent antibacterial properties. Notably, the higher the content of Cu-AC in the composites, the more effective the antibacterial effect, with an antibacterial rate of over 90% being achieved at a copper content of 300 ppm and over 99% at 700 ppm. Moreover, the effects of Cu-AC on the thermal degradability, processability and mechanical properties of typical thermoplastic PP were systematically investigated. The results indicate that the interaction between the dual functionalized Cu-AC and PP molecular chains leads to a reduction of the viscosity and modulus of PP, and improves the processability, thermal stability and mechanical properties of PP. Overall, the outstanding antimicrobial properties of copper nanoparticles and the ease of processing and improved thermal/mechanical performance of their antibacterial thermoplastic composites make them highly versatile, holding great promise for future applications in various industries, such as protection, breeding, building materials, home appliances, and more.

Author contributions

Lulu Tian: investigation, formal analysis, data curation, and writing – original draft. Li Sun: investigation and data curation. Bo Gao: investigation and data curation. Fei Li: investigation and data curation. Chaoran Li: investigation and performance analysis. Ruoyu Wang: methodology and resources. Yanfang Liu: methodology and resources. Xiaohong Li: conceptualization, methodology, and visualization. Liyong Niu: conceptualization, methodology, visualization, and writing – review and editing. Zhijun Zhang: conceptualization, methodology, and visualization. All authors read and contributed to the manuscript.

Conflicts of interest

There are no conflicts to declare.

Acknowledgements

This work was financially supported by the Key Research and Development Program of Henan Province (Grant No. 221111230100), the Science and Technology Development Plan of Henan Province (Grant No. 222102230051) and the Graduate Education Innovation and Quality Enhancement Project of Henan University (Grant No. SYLJD2023003).

References

1 K. Hoelzer, A. I. Moreno Switt, M. Wiedmann and K. J. Boor, *Food Microbiol.*, 2018, **75**, 65–71.
2 T. F. Jones and J. Yackley, *Foodborne Pathog. Dis.*, 2018, **15**, 11–15.
3 D. Belina, Y. Hailu, T. Gobena, T. Hald and P. M. K. Njage, *One Health Outlook*, 2021, **3**, 19.
4 F. Fung, H. S. Wang and S. Menon, *Biomed. J.*, 2018, **41**, 88–95.
5 L. Chen and W. Alali, *Front. Microbiol.*, 2018, **9**, 2412.
6 L. Lozica, C. S. Morteza Gholi, A. Kela, I. Losic, D. Horvatek Tomic and Z. Gottstein, *Vaccines*, 2022, **10**, 1567.
7 S. Saidin, M. A. Jumat, N. A. A. Mohd Amin and A. S. Saleh Al-Hammadi, *Mater. Sci. Eng., C*, 2021, **118**, 111382.
8 K. Zhang, X. Li, M. Nie and Q. Wang, *Compos. Sci. Technol.*, 2018, **158**, 121–127.
9 E. G. A. Owusu, E. Yaghini, I. Naasani, I. P. Parkin, E. Allan and A. J. MacRobert, *Nanoscale*, 2020, **12**, 10609–10622.
10 X. Zhu, Y. Zhu, K. Jia, B. S. Abraha, Y. Li, W. Peng, F. Zhang, X. Fan and L. Zhang, *Nanoscale*, 2020, **12**, 19129–19141.
11 Y. P. Wang, Q. Q. Wang, G. Y. Wu, H. X. Xiang, M. T. Innocent, M. Zhai, C. Jia, P. Zou, J. L. Zhou and M. F. Zhu, *J. Mater. Sci. Technol.*, 2022, **122**, 1–9.
12 M. Vincent, P. Hartemann and M. Engels-Deutsch, *Int. J. Hyg. Environ. Health*, 2016, **219**, 585–591.
13 H. Xu, D. Liu, Y. Song, Y. Xie, Z. Shi, C. Xiong and Q. Yang, *Compos. Sci. Technol.*, 2022, **228**, 109679.
14 J. Chen, L. Fan, C. Yang, S. Wang, M. Zhang, J. Xu and S. Luo, *Int. J. Biol. Macromol.*, 2020, **161**, 1286–1295.
15 G. Q. Gu, C. B. Han, J. J. Tian, C. X. Lu, C. He, T. Jiang, Z. Li and Z. L. Wang, *ACS Appl. Mater. Interfaces*, 2017, **9**, 11882–11888.

16 D. Sun, J. Turner, N. Jiang, S. Zhu, L. Zhang, B. G. Falzon, C. P. McCoy, P. Maguire, D. Mariotti and D. Sun, *Compos. Sci. Technol.*, 2020, **186**, 107911.
17 Y. Seo, J. Hwang, E. Lee, Y. J. Kim, K. Lee, C. Park, Y. Choi, H. Jeon and J. Choi, *Nanoscale*, 2018, **10**, 15529–15544.
18 F. Beigmohammadi, S. H. Peighambardoust, J. Hesari, S. Azadmard-Damirchi, S. J. Peighambardoust and N. K. Khosrowshahi, *LWT – Food Sci. Technol.*, 2016, **65**, 106–111.
19 D. Mitra, E. T. Kang and K. G. Neoh, *ACS Appl. Mater. Interfaces*, 2020, **12**, 21159–21182.
20 H. f. Chen, J. j. Wu, M. y. Wu and H. Jia, *New Carbon Mater.*, 2019, **34**, 382–389.
21 B. L. España-Sánchez, C. A. Ávila-Orta, F. Padilla-Vaca, M. G. Neira-Velázquez, P. González-Morones, J. A. Rodríguez-González, E. Hernández-Hernández, Á. Rangel-Serrano, E. D. Barriga-C, L. Yate and R. F. Ziolo, *Plasma Processes Polym.*, 2014, **11**, 353–365.
22 Z. Q. Yang, X. P. Hao, S. G. Chen, Z. Q. Ma, W. H. Wang, C. Y. Wang, L. F. Yue, H. Y. Sun, Q. Shao, V. Murugadoss and Z. H. Guo, *J. Colloid Interface Sci.*, 2019, **533**, 13–23.
23 X. Y. Ye, Y. Chen, J. Yang, H. Y. Yang, D. W. Wang, B. B. Xu, J. N. Ren, D. Sridhar, Z. H. Guo and Z. J. Shi, *Adv. Compos. Hybrid Mater.*, 2023, **6**, 106.
24 G. Gautam and P. Mishra, *J. Food Process. Preserv.*, 2017, **41**, 13243.
25 M. B. Gawande, A. Goswami, F. X. Felpin, T. Asefa, X. Huang, R. Silva, X. Zou, R. Zboril and R. S. Varma, *Chem. Rev.*, 2016, **116**, 3722–3811.
26 M. Bhagat, R. Anand, P. Sharma, P. Rajput, N. Sharma and K. Singh, *ECS J. Solid State Sci. Technol.*, 2021, **10**, 063011.
27 F. Parveen, B. Sannakki, M. V. Mandke and H. M. Pathan, *Sol. Energy Mater. Sol. Cells*, 2016, **144**, 371–382.
28 F. Liu, C. Y. Hu, Q. Zhao, Y. J. Shi and H. N. Zhong, *Food Addit. Contam.: Part A*, 2016, **33**, 1741–1749.
29 G. Naikoo, F. Al-Mashali, F. Arshad, N. Al-Maashani, I. U. Hassan, Z. Al-Baraami, L. H. Faruck, A. Qurashi, W. Ahmed, A. M. Asiri, A. A. Aljabali, H. A. Bakshi and M. M. Tambuwala, *Curr. Pharm. Des.*, 2021, **27**, 4416–4432.
30 K. S. Tan and K. Y. Cheong, *J. Nanopart. Res.*, 2013, **15**, 1537.
31 Y. Xue, Z. Zhao, Y. Zhao, C. Wang, S. Shen, Z. Qiu, R. Cui, S. Zhou, L. Fang, Z. Chen, H. Zhu and B. Zhu, *Nanoscale*, 2022, **14**, 12789–12803.
32 I. Lee, J. Roh, J. Lee, J. Song and J. Jang, *Polymer*, 2016, **83**, 223–229.
33 J. Vieillard, N. Bouazizi, M. N. Morshed, T. Clamens, F. Desriac, R. Bargougui, P. Thebault, O. Lesouhaitier, F. Le Derf and A. Azzouz, *Ind. Eng. Chem. Res.*, 2019, **58**, 10179–10189.
34 Y. Qian, S. Deng, Z. Cong, H. Zhang, Z. Lu, N. Shao, S. A. Bhatti, C. Zhou, J. Cheng, S. H. Gellman and R. Liu, *J. Am. Chem. Soc.*, 2022, **144**, 1690–1699.
35 B. V. Lingesh, B. N. Ravi Kumar, B. M. Rudresh and H. N. Reddappa, *Adv. Compos. Hybrid Mater.*, 2018, **1**, 766–776.
36 H. Palza, *Int. J. Mol. Sci.*, 2015, **16**, 2099–2116.
37 Y. Zhu, Y. Wang, L. Sha and J. Zhao, *Appl. Surf. Sci.*, 2017, **425**, 1101–1110.
38 I. Salah, I. P. Parkin and E. Allan, *RSC Adv.*, 2021, **11**, 18179–18186.
39 L. Tamayo, M. Azocar, M. Kogan, A. Riveros and M. Paez, *Mater. Sci. Eng., C*, 2016, **69**, 1391–1409.
40 A. Ghazzy, R. R. Naik and A. K. Shakya, *Polymers*, 2023, **15**, 2167.
41 J. Y. Kim, D. Hong, J. C. Lee, H. G. Kim, S. Lee, S. Shin, B. Kim, H. Lee, M. Kim, J. Oh, G. D. Lee, D. H. Nam and Y. C. Joo, *Nat. Commun.*, 2021, **12**, 3765.
42 P. Zhao, H. Jiang, H. Shen, S. Yang, R. Gao, Y. Guo, Q. Zhang and H. Zhang, *Angew. Chem.*, 2023, e202314121.
43 D. Auhl, F. J. Stadler and H. Münstedt, *Macromolecules*, 2012, **45**, 2057–2065.
44 A. Roy and M. Joshi, *Polym. Int.*, 2018, **67**, 917–924.
45 L. Pan, X. Wang, C. Lu, J. Chen, K. Huang, M. Xiao, L. Chen and F. Chen, *Eng. Plast. Appl.*, 2020, **48**, 57–62.
46 M. Yang, J. Li and W. Xie, *J. Wuhan Univ. Technol., Mater. Sci. Ed.*, 2018, **33**, 749–757.
47 M. C. Han, H. W. He, W. K. Kong, K. Dong, B. Y. Wang, X. Yan, L. M. Wang and X. Ning, *Fibers Polym.*, 2022, **23**, 1947–1955.
48 X. Fang, J. Lang, H. Song, L. Wang and J. Bian, *Packag. Eng.*, 2021, **42**, 157–164.